
BCONFORMER: A CONFORMER BASED ON MUTUAL SAMPLING FOR UNIFIED PREDICTION OF CONTINUOUS AND DISCONTINUOUS ANTIBODY BINDING SITES

Zhangyu You*,
College of Life Sciences
Sichuan University
Chengdu

2022141240189@stu.scu.edu.cn

Jiahao Ma*,
Material Innovation Institute for Life Sciences and Energy
The University of Hong Kong
Hetao SZ-HK Cooperation Zone
jiahao.ma@connect.hku.hk

Hongzong Li*,
Hong Kong Generative AI Research and Development Center
The Hong Kong University of Science and Technology
Hong Kong
lihongzong@ust.hk

Ye-Fan Hu*[†],
Computational Immunology Centre
BayVax Biotech Limited
Hong Kong
yefan.hu@bayvaxbio.com

Jian-Dong Huang[†]
School of Biomedical Sciences
The University of Hong Kong
Hong Kong
jdhuang@hku.hk

ABSTRACT

Accurate prediction of antibody-binding sites (epitopes) on antigens is crucial for vaccine design, immunodiagnostics, therapeutic antibody development, antibody engineering, research into autoimmune and allergic diseases, and for advancing our understanding of immune responses. Despite *in silico* methods that have been proposed to predict both linear (continuous) and conformational (discontinuous) epitopes, they consistently underperform in predicting conformational epitopes. In this work, we propose a conformer-based model trained on antigen sequences derived from 1,080 antigen-antibody complexes, leveraging convolutional neural networks (CNNs) to extract local features and Transformers to capture long-range dependencies within antigen sequences. Ablation studies demonstrate that CNN enhances the prediction of linear epitopes, and the Transformer module improves the prediction of conformational epitopes. Experimental results show that our model outperforms existing baselines in terms of PCC, ROC-AUC, PR-AUC, and F1 scores on conformational epitopes.

Keywords B-cell Epitope Prediction; Conformer; Antigen–Antibody Interface

1 Introduction

B cells are key effectors of the adaptive immune system, coordinating responses to pathogenic and aberrant signals. Each B cell expresses a single clonotype of B-cell receptor (BCR), a membrane-bound antibody that interacts with specific antigens. The binding sites on the antigen—known as the epitope—can be linear (continuous) or conformational (discontinuous), and the corresponding binding sites on the antibody are called paratopes. Linear epitopes are formed by

*Equal contribution.

[†]Corresponding authors.

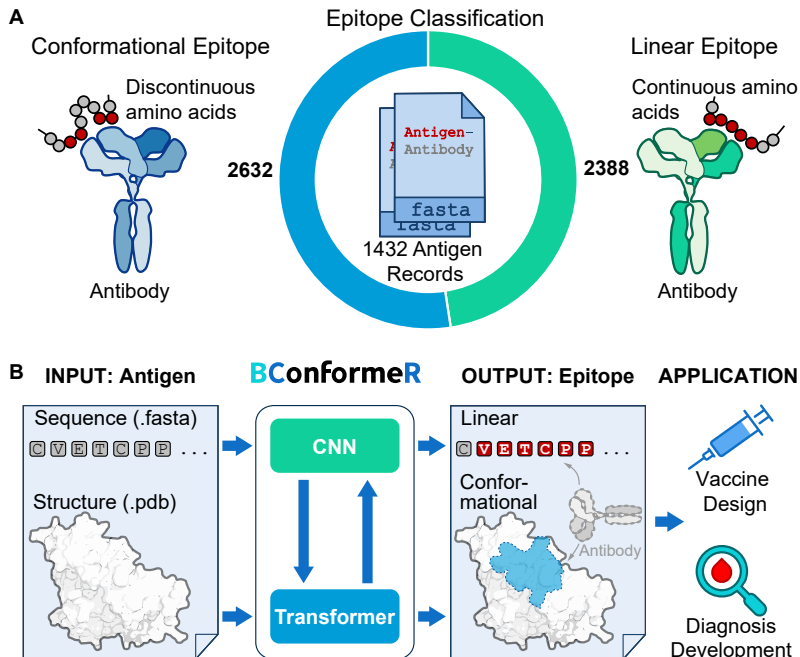


Figure 1: Overview of epitope classification and BConformerR prediction. (A) Epitopes, i.e., Antibody-binding sites, include conformational fragments ($n=2,632$) and linear regions ($n=2,388$). Data derived from 1,432 antigen records. (B) Epitope prediction workflow: Antigen inputs are processed to predict linear and conformational epitopes, which enable applications in vaccine design and diagnostic development.

linear stretches of amino acid residues, while conformational epitopes are formed by distant residues brought together in 3D through folding.

Identifying epitopes is critical for antibody engineering [1, 2], disease diagnosis [3, 4], and vaccine optimization [5, 6]. Experimental techniques such as X-ray crystallography and cryo-electron microscopy provide high-resolution antigen-antibody (Ag-Ab) interactions but are resource-intensive [7, 8]. Phage display is faster but lacks atomic-level precision [9]. Therefore, many *in silico* methods have been developed to predict epitopes.

Sequence-based methods such as SEMA-1D [10, 11], BepiPred [12, 13, 14] and SEPPA [15] are widely used due to the availability of antigen sequences, with SEMA-1D 2.0 [11] and BepiPred-3.0 [14] notably improving performance by incorporating representations from the protein language model ESM-2 [16, 17]. Structure-based methods, such as SEMA-3D [10, 11], DiscoTope [18, 19], ScanNet [20] and Epitope3D [21], take the residue geometry and surface accessibility into consideration, but remain constrained by the limited availability of high-quality antigen structures. Among these methods, DiscoTope-3.0 [19] achieves the best performance in the benchmark evaluation.

However, epitope prediction remains a challenging task, with existing methods underperform on conformational ones. Moreover, there is a lack of hybrid backbone models to effectively handle both linear and conformational epitopes. A key source of this complexity stems from the nature of Ag-Ab interfaces, where linear epitopes are clustered along the sequence, and conformational epitopes are often spatially proximate but dispersed across different regions of the linear sequence [22]. To address this multi-scale complexity, we designed the Conformer architecture, which integrates convolution layers to learn local residue-level features and self-attention mechanisms to capture long-range dependencies within antigen sequences [23, 24].

Here, we propose **BConformerR**, a **Conformer**-based model for linear and conformational **BCR** epitope prediction. Antigen sequences from 1,180 Ag-Ab complexes were embedded using ESM-2, with 1,080 used for training and 100 for evaluation. In a blind test of 24 antigen records, BConformerR outperforms existing baselines—SEPPA-3.0, BepiPred-3.0, SEMA-1D 2.0 and DiscoTope-3.0—across multiple metrics, including PCC, ROC-AUC, PR-AUC, and F1 score on conformational epitopes. To further dissect the model’s design, we ablated ResNet bottlenecks and ViT modules from Conformer, showing that convolutional layers improve linear epitope prediction, and Transformer modules are critical for capturing discontinuous epitope patterns.

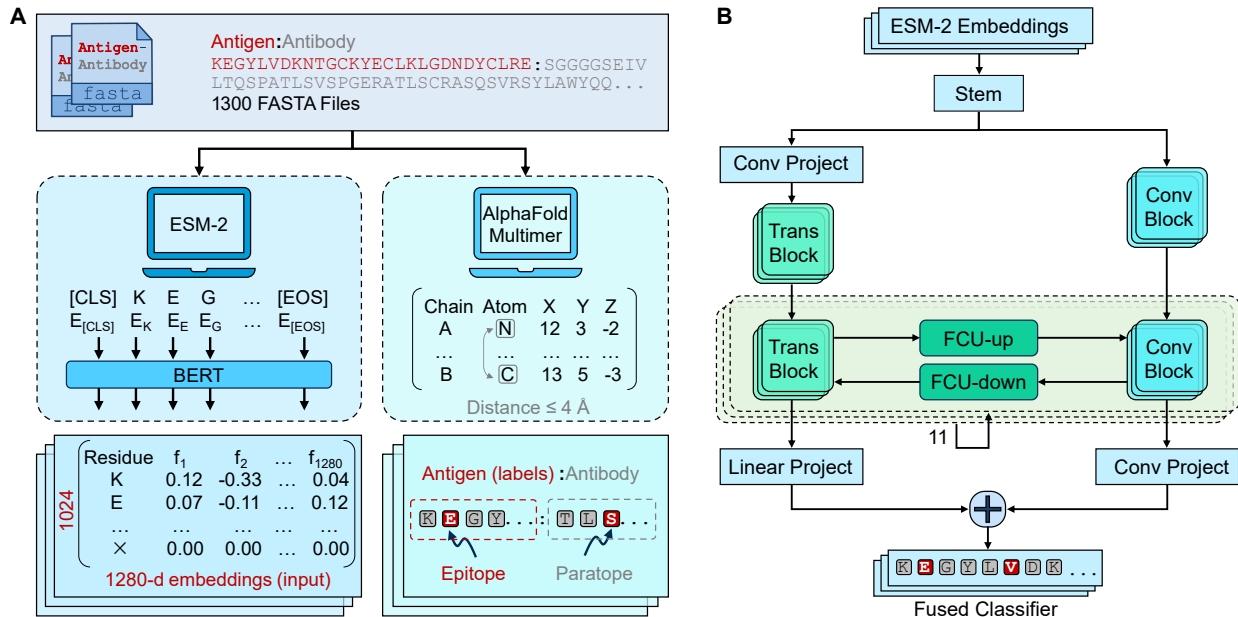


Figure 2: BConformer overview. (A) Preparation pipeline of the data. 1300 antigen-antibody FASTA files were processed using AlphaFold Multimer v3 to predict structures, with top-ranked structure for each was selected to extract epitopes (right); Antigen sequences were embedded by ESM-2, producing embeddings of dimension 1024×1280 (left). (B) Conformer architecture. Stem module applies convolution and max-pooling to the original ESM-2 embeddings; The Conv block and Trans block are based on ResNet bottleneck and Vision Transformer modules respectively; Feature coupling units (FCU-Up and FCU-Down) connect the Conv and Trans blocks, with 11 FCU layers in total; The classifier linearly fuses features from both Conv and Trans branches.

2 Related Work

2.1 Antibody-agnostic prediction models

Numerous models, trained on antigen-epitope pairs, have been proposed and refined to enhance epitope prediction. SEPPA-3.0 was the epitope prediction tool specifically designed for glycoproteins, based on the logistic regression classifier [15]. BepiPred-3.0 used embeddings from pretrained protein language models ESM-2 as input to a feedforward neural network (FFNN) to predict both linear and conformational B-cell epitopes [14]. Epitope3D modeled antigen surfaces as residue-level graphs and extracted distance-based graph signatures to train classifiers for conformational B-cell epitope prediction, with AdaBoost selected as the backbone [21, 25]. ScanNet was an end-to-end geometric deep learning model that learned interpretable residue-level features directly from 3D structural neighborhoods [20]. SEMA-1D 2.0 was constructed by adding a fully-connected linear layer on an ensemble of five ESM-2 models, while SEMA-3D 2.0 was developed using an ensemble of five pre-trained Structure-aware Protein language models (SaProt) [11, 26]. DiscoTope-3.0 utilized inverse folding representations from ESM-IF1 and was trained on both predicted and solved structures using a positive-unlabelled ensemble strategy, enabling structure-based B-cell epitope prediction at scale [19, 27].

However, existing models rarely incorporate both local features and long-range dependencies within antigen sequences, showing limited performance on conformational epitopes. Therefore, we adopted a Conformer based on mutual sampling, employing CNNs to extract local features and Transformers to capture long-range dependencies within antigen sequences.

2.2 Antibody-aware evaluation models

Despite advances in epitope prediction, evaluating Ag-Ab binding confidence remains challenging, which is crucial for vaccine selection. AbEpitope-1.0, a recent method for predicting antibody targets by use of AlphaFold and inverse folding, significantly improving the prediction accuracy of Ag-Ab interfaces. They constructed negative Ag-Ab samples (false binding pairs) by swapping antibody chains across real complexes in the dataset. Each sample was labeled

as either true or false to train the model to distinguish authentic Ag-Ab interactions from decoys. The final model, AbEpiTarget-1.0, achieved superior performance in antibody-sensitive scoring for target prediction [28].

In this work, we utilize the real Ag-Ab complex dataset provided by AbEpiTope-1.0, employing its epitope identification pipeline to ensure the data quality (Fig. 2A).

3 Method

3.1 Epitope Extraction

3.1.1 Epitope identification

During immune recognition, epitopes are typically composed of multiple spatially adjacent residues. To capture this interaction, the notions of residue-neighbor and residue-patch were introduced. A residue-neighbor is defined when the minimum distance between any atoms of two residues is less than 4 Å, and a residue-patch refers to a group of residues whose atoms lie within 10 Å of a central residue [29]. In our study, we focused on the residue-neighbor relationship to capture the tight spatial interactions, which is given as:

$$\min_{a \in r_i, b \in r_j} \|a - b\| < 4 \text{ \AA}, \quad (1)$$

where r_i and r_j are residues from the antigen and antibody chains respectively, and a, b represent the heavy atoms within these residues.

3.1.2 Epitope classification

Generally, epitopes are separated into multiple Regions (R) and Fragments (F) for each antigen sequence. Regions are defined as linear stretches of antigen sequence having at least three antibody-contacting residues. Gaps between contacting residues are allowed, and a gap size of up to three non-contacting residues is chosen on the basis of the structure of α -helices, which enables residues on the same helical face to be included [30]. Fragments, which do not contain enough antibody-contacting residues to qualify as a region, are considered discontinuous in our study (Fig. 1A).

For real and predicted annotations, linear and discontinuous epitopes are extracted from regions and fragments, respectively. Ambiguous cases occur when the real and predicted labels differ, especially when a residue is annotated as part of a region in the ground truth but as part of a fragment in the prediction, or vice versa. To address this, all classifications are determined based on the ground-truth labels. That is, for a real label $r \in \{N, L, D\}$ and predicted label $p \in \{N, L, D\}$, the final classification $c(r, p)$ is defined as:

$$c(r, p) = \begin{cases} L, & (r, p) \in \{(L, \cdot), (N, L)\} \\ D, & (r, p) \in \{(D, \cdot), (N, D)\} \\ N, & (r, p) = (N, N) \end{cases} \quad (2)$$

where N, L , and D denote non-epitope, linear epitope and discontinuous epitope, respectively. Performance metrics (e.g., F1) are then calculated for each type of epitopes.

3.2 Conformer

3.2.1 Overview

To take advantage of both local and global representations for epitope prediction, we construct BConformerR, a dual-branch architecture adapted from Conformer [24], as shown in Table 1. BConformerR consists of a shared convolutional stem, a CNN branch, a Transformer branch, Feature Coupling Units (FCUs) for bidirectional feature exchange, and two per-position classifiers (Fig. 2B). Since our task is per-residue epitope prediction, all antigen sequences are padded to a fixed length of L (e.g., 1024) and this length is preserved throughout the model.

The stem consists of a 1D convolution (kernel size 7) and a 1D max pooling (kernel size 3), designed to capture contextual features for each residue. And the embedding dimension C (e.g., 1280) is reduced to $C/4$ channels after the stem. In the first block, both branches process identical initial features and therefore no feature coupling is applied. From the second block onward, FCUs are inserted to progressively fuse local and global representations. The input is processed by alternating CNN and Transformer blocks, where at each stage, CNN-derived local features are passed to the Transformer branch, and Transformer-derived global representations are fed back to the CNN branch. The CNN

stage	output	CNN Branch	FCU	Transformer Branch
stem	1024	7, 320		
		3 max pooling		
s1	1024	$\begin{bmatrix} 1, 160 \\ 3, 160 \\ 1, 640 \end{bmatrix}$	-	$\begin{bmatrix} 5, 1536 \\ \text{MHSA-12, 1536} \\ 1, 3072 \\ 1, 1536 \end{bmatrix} \times 1$
		$\begin{bmatrix} 1, 160 \\ 3, 160 \\ 1, 640 \end{bmatrix}$	$[1, 1536] \rightarrow$	$\begin{bmatrix} \text{MHSA-12, 1536} \\ 1, 3072 \\ 1, 1536 \end{bmatrix} \times 3$
	$\begin{bmatrix} 1, 160 \\ 3, 160 \\ 1, 640 \end{bmatrix}$	$\leftarrow [1, 160]$		
s2	1024	$\begin{bmatrix} 1, 320 \\ 3, 320 \\ 1, 1280 \end{bmatrix}$	$[1, 1536] \rightarrow$	$\begin{bmatrix} \text{MHSA-12, 1536} \\ 1, 3072 \\ 1, 1536 \end{bmatrix} \times 4$
		$\begin{bmatrix} 1, 320 \\ 3, 320 \\ 1, 1280 \end{bmatrix}$	$\leftarrow [1, 320]$	
s3	1024	$\begin{bmatrix} 1, 640 \\ 3, 640 \\ 1, 2560 \end{bmatrix}$	$[1, 1536] \rightarrow$	$\begin{bmatrix} \text{MHSA-12, 1536} \\ 1, 3072 \\ 1, 1536 \end{bmatrix} \times 4$
		$\begin{bmatrix} 1, 640 \\ 3, 640 \\ 1, 2560 \end{bmatrix}$	$\leftarrow [1, 640]$	
classifier	1024	$2560 \rightarrow 2$	-	$1536 \rightarrow 2$
		$\alpha \times \text{Conv}_{\text{cls}} + (1 - \alpha) \times \text{Trans}_{\text{cls}}$		

Table 1: Architecture of BConformer, a 1D adaptation of Conformer [24]. The MHSA-12 indicates multi-head self-attention with 12 heads operating on 1536-dimensional embeddings (128 dimensions per head). Conv_{cls} denotes the 1D convolutional classifier operating on CNN features, and $\text{Trans}_{\text{cls}}$ denotes the linear classifier operating on Transformer outputs. The final prediction is obtained by a weighted fusion of the two.

branch gradually expands to $2C$ channels, and the Transformer branch maintains D -dimensional (e.g., 1536) token embeddings at the end.

Finally, a 1D convolutional classifier and a linear classifier are applied to the outputs of the CNN and Transformer branches, respectively, producing per-residue logits $\mathbf{y}_{\text{CNN}}, \mathbf{y}_{\text{Trans}} \in \mathbb{R}^{L \times 2}$. These are linearly fused and converted to per-residue class probabilities using the softmax function:

$$\mathbf{p}_i = \text{softmax}(\alpha \mathbf{y}_{\text{CNN},i} + (1 - \alpha) \mathbf{y}_{\text{Trans},i}), \quad (3)$$

where $\mathbf{y}_i \in \mathbb{R}^2$ denotes the logits for the i -th residue, and α is the weighted parameter.

3.2.2 CNN branch

The CNN branch is composed of three stages after the stem, each consisting of repeated convolutional blocks based on the ResNet bottleneck design [31]. Given an input feature sequence $\mathbf{x} \in \mathbb{R}^{C' \times L}$, a bottleneck performs three sequential convolutions with a residual connection applied to \mathbf{x} :

$$\begin{aligned} \mathbf{z}_1 &= \sigma(\text{BN}_1(\text{Conv}_{1 \times 1}(\mathbf{x}))), \\ \mathbf{z}_2 &= \sigma(\text{BN}_2(\text{Conv}_{3 \times 1}(\mathbf{z}_1))), \\ \mathbf{z}_3 &= \text{BN}_3(\text{Conv}_{1 \times 1}(\mathbf{z}_2)), \\ \mathbf{y} &= \sigma(\mathbf{z}_3 + \mathcal{F}(\mathbf{x})), \end{aligned} \quad (4)$$

where $\sigma(\cdot)$ denotes the ReLU activation, BN represents 1D batch normalization, and

$$\mathcal{F}(\mathbf{x}) = \begin{cases} \mathbf{x}. & \text{if shape matches} \\ \text{BN}_{\text{res}}(\text{Conv}_{1 \times 1}(\mathbf{x})). & \text{otherwise} \end{cases}$$

The channel dimension is first downsampled to half, then expanded by a factor of 4 within each bottleneck. The first convolution block contains a single bottleneck, while subsequent blocks include two bottlenecks: one applied before the Transformer branch, and the other afterward. Since convolution kernels slide over representation sequences with overlap, the CNN blocks are well-suited to capture residue-level contextual information, providing local features for the Transformer branch.

3.2.3 Transformer branch

The Transformer branch processes residue embeddings using 12 repeated Transformer blocks. Each block follows the standard architecture introduced in ViT [32], but adapted to 1D protein sequences. As shown in Table 1, each block contains a multi-head self-attention module and a two-layer feed-forward MLP block. Both submodules are preceded by Layer Normalization (LN) with residual connections. Specifically, given the input sequence $\mathbf{x} \in \mathbb{R}^{L \times D}$, a single Transformer block updates the representation as follows:

$$\begin{aligned} \mathbf{z}_1 &= \mathbf{x} + \text{DropPath}(\text{MHSA}(\text{LN}_1(\mathbf{x}))), \\ \mathbf{z}_2 &= \mathbf{z}_1 + \text{DropPath}(\text{MLP}(\text{LN}_2(\mathbf{z}_1))), \end{aligned} \quad (5)$$

where $\text{MHSA}(\cdot)$ denotes the multi-head self-attention mechanism with h (e.g., 12) heads, and $\text{MLP}(\cdot)$ consists of a linear up-projection to $2D$ dimensions, a GELU activation, followed by a linear down-projection to D . The DropPath operator implements stochastic depth regularization.

Since the CNN branch already encodes positional information, no explicit positional embeddings are added. Also, we omit the use of [CLS] tokens as our task is residue-level classification. This branch facilitates the modeling of long-range interactions between residues, preserving spatial information of discontinuous epitopes.

3.2.4 Feature coupling units

To enable bidirectional interaction between the local CNN features and global Transformer representations, we introduce FCUs starting from the second block. FCUs consist of two modules: FCU-Down, which passes CNN features to the Transformer; and FCU-Up, which feeds Transformer outputs back to the CNN.

FCU-Down projects the CNN features $\mathbf{F}_{\text{CNN}} \in \mathbb{R}^{C_1 \times L}$ into the Transformer embedding space $\mathbb{R}^{L \times D}$ via a 1×1 convolution and batch normalization, followed by transposition to align the dimensions. The projected features $\mathbf{F}_{\text{CNN}}^{\rightarrow}$ are then added to the Transformer input $\mathbf{F}_{\text{Trans}}$:

$$\begin{aligned} \mathbf{F}_{\text{CNN}}^{\rightarrow} &= (\text{BN}(\text{Conv}_{1 \times 1}(\mathbf{F}_{\text{CNN}})))^T, \\ \tilde{\mathbf{F}}_{\text{Trans}} &= \mathbf{F}_{\text{Trans}} + \mathbf{F}_{\text{CNN}}^{\rightarrow}. \end{aligned} \quad (6)$$

FCU-Up maps the Transformer features $\tilde{\mathbf{F}}_{\text{Trans}} \in \mathbb{R}^{L \times D}$ back to the CNN feature space $\mathbb{R}^{C_2 \times L}$ by transposing first, then applying a 1×1 convolution and batch normalization. The transformed features $\mathbf{F}_{\text{Trans}}^{\leftarrow}$ are added to the original CNN features \mathbf{F}_{CNN} :

$$\begin{aligned} \mathbf{F}_{\text{Trans}}^{\leftarrow} &= \text{BN}(\text{Conv}_{1 \times 1}(\tilde{\mathbf{F}}_{\text{Trans}}^T)), \\ \tilde{\mathbf{F}}_{\text{CNN}} &= \mathbf{F}_{\text{CNN}} + \mathbf{F}_{\text{Trans}}^{\leftarrow}. \end{aligned} \quad (7)$$

3.3 Performance Metric

3.3.1 AgIoU

To evaluate the overlap between the prediction and real epitopes, we use the Antigen-level Intersection over Union (AgIoU), which is defined as the ratio of the number of correctly predicted epitope residues to the total number of residues that are either labeled as epitope in the ground truth or prediction as such:

$$\text{AgIoU} = \frac{\text{Res}_{\text{true}} \cap \text{Res}_{\text{pred}}}{\text{Res}_{\text{true}} \cup \text{Res}_{\text{pred}}}. \quad (8)$$

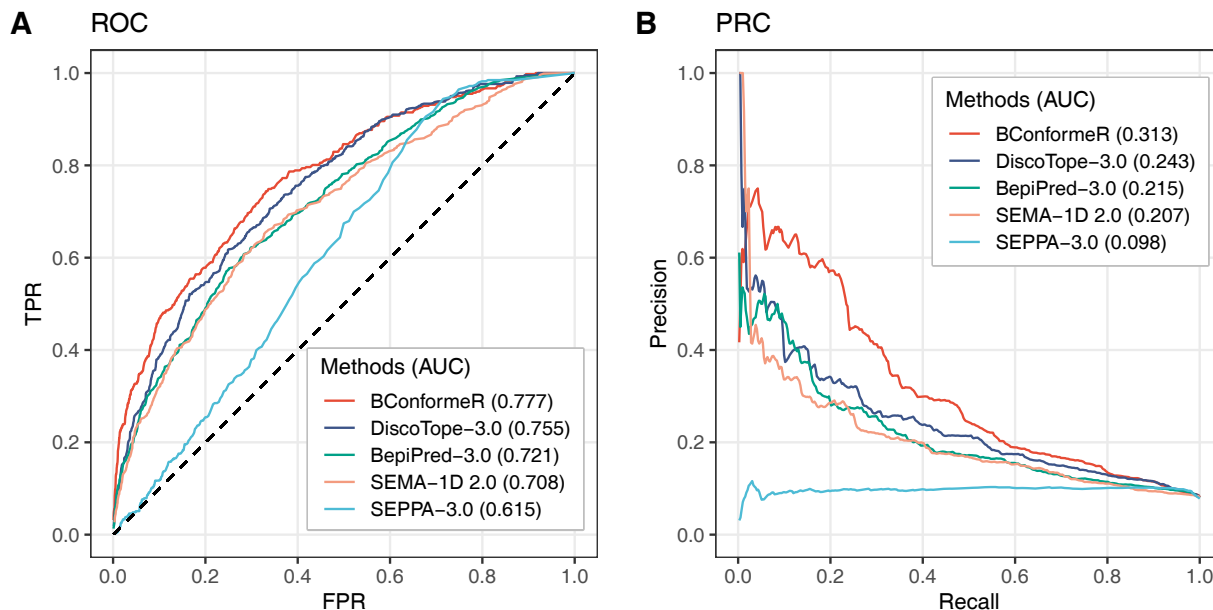


Figure 3: Improved performance on epitope prediction. ROC-AUC and PR-AUC curves plot on the blind test set of 24 antigen records. (A) ROC-AUC curves. (B) PR-AUC curves.

Method	Threshold	F1-L \uparrow	F1-D \uparrow	MCC \uparrow	PCC \uparrow	AgIoU \uparrow
SEPPA-3.0	0.100 \pm 0.020	0.606 \pm 0.055	0.024 \pm 0.001	0.058 \pm 0.014	0.067	0.088 \pm 0.005
BepiPred-3.0	0.210 \pm 0.020	0.657 \pm 0.032	0.034 \pm 0.003	0.191 \pm 0.003	0.215	0.149 \pm 0.003
SEMA-1D 2.0	0.510 \pm 0.030	0.683 \pm 0.027	0.029 \pm 0.001	0.182 \pm 0.002	0.217	0.143 \pm 0.002
DiscoTope-3.0	0.300 \pm 0.020	0.706 \pm 0.015	0.047 \pm 0.003	0.227 \pm 0.007	0.276	0.167 \pm 0.002
BConformeR	0.300 \pm 0.020	0.673 \pm 0.014	0.105 \pm 0.004	0.302 \pm 0.003	0.347	0.212 \pm 0.002

Table 2: Performance comparison of different methods on a blind test of 24 antigen records. F1-L and F1-D refer to the F1 scores calculated on linear and discontinuous epitopes, respectively; Thresholds were selected following those of baseline methods; Standard deviation calculated over a range of thresholds.

4 Experiments

4.1 Experiments Setup

4.1.1 Dataset

We collected 1,300 Ab–Ag complex FASTA files with AlphaFold-2.3 colabfold version from AbEpiTope-1.0. Each complex was then modeled with AlphaFold2 Multimer v3, generating 30 structural predictions per complex and a total of 39,000 structures. For each complex, we selected the top-ranked model and excluded those with a pLDDT score below 0.82. Interface residues were extracted based on a distance cutoff of 4 Å between heavy atoms on the antigen and antibody chains (1). To enhance data quality and limit parameter overhead, we removed complexes containing insufficient epitope residues or antigens exceeding 1024 residues in length. Finally, the dataset contains 1,180 Ag-Ab complexes in total: 1,080 used for training BConformeR, and 100 set aside for evaluation and ablation. And the antigen chains annotated with epitope labels serve as the input.

Due to the differences in training and test datasets across existing epitope prediction methods, the selection of a blind test set was important for fair evaluation. Therefore, we also extracted 24 antigen records from the test sets of SEMA-1D 2.0 and DiscoTope-3.0. At least 75% of these records were previously used as test data by each baseline method, and 100% blind for BConformeR.

Model	Linear			Discontinuous			Params (M)	MACs (G)
	Precision	Recall	F1	Precision	Recall	F1		
Conformer-12	0.965	0.516	0.672	0.064	0.393	0.110	302.24	309.93
Conformer-9	0.946	0.489	0.645(-4.0%)	0.055	0.344	0.095(-13.6%)	230.27	236.12
Conformer-6	0.977	0.449	0.615(-8.5%)	0.041	0.263	0.071(-35.5%)	158.30	162.31
ResNet-152	0.979	0.514	0.674(+0.3%)	0.046	0.290	0.079(-28.2%)	242.44	248.62
ResNet-101	0.961	0.468	0.629(-6.4%)	0.027	0.216	0.048(-56.4%)	179.24	183.80
ViT-12	0.969	0.477	0.639(-4.9%)	0.049	0.355	0.086(-21.8%)	230.24	234.42
ViT-9	0.958	0.455	0.617(-8.2%)	0.047	0.328	0.082(-25.5%)	173.57	176.32

Table 3: Ablation study of different models evaluated on 100 antigen records. Conformer-12 corresponds to BConformerR, and Conformer-9/6 reduces one layer of FCU-based CNN and Transformer for each stage compared to Conformer-12/9. ResNet bottlenecks adopt the same CNN blocks as used in Conformer, and ViT follows the design of Transformer branch. Models are grouped with comparable Params and MACs: Conformer-9, ResNet-152 and ViT-12; Conformer-6, ResNet-101 and ViT-9.

4.1.2 Data encodings and features

To represent antigen sequences, we used pretrained ESM-2 embeddings. Sequences were tokenized with the ESM-2 tokenizer and passed through its 33-layer transformer. We extracted the hidden states from the final layer, discarded the beginning-of-sequence (BOS) and end-of-sequence (EOS) tokens, and retained only the embeddings corresponding to the actual residues. Finally, each antigen sequence was represented as a $\mathbb{R}^{1024 \times 1280}$ feature matrix, with 1024 as the padded length and 1280 as the ESM-2 embedding size.

4.2 Comparison with SOTA Methods

4.2.1 Benchmark evaluation

The performance of BConformerR was evaluated on a blind test set of 24 antigen records and compared with four SOTA methods: SEPPA-3.0, BepiPred-3.0, SEMA-1D 2.0 and DiscoTope-3.0. As shown in Table 2, BConformerR outperforms baselines in MCC (0.302), PCC (0.347), and AgIoU (0.212). Further evaluation of ROC-AUC and PR-AUC shows that BConformerR achieves scores of 0.777 and 0.313 respectively, surpassing all methods that provided residue-level probabilistic outputs (Fig. 3).

4.2.2 Enhanced prediction on conformational epitopes

To evaluate the ability of each method in predicting linear and conformational epitopes, we computed the F1 scores separately on the test set. As shown in Table 2, BConformerR achieves an F1 score of 0.105 on discontinuous epitopes, significantly higher than baseline methods that typically report these scores below 0.050. This illustrates that BConformerR is more effective at identifying non-contiguous epitope fragments.

4.3 Ablation

4.3.1 Overview

To further assess the contribution of each module to linear and conformational epitope prediction, we ablated the dual-branch Conformer into standalone ResNet and ViT variants. We first reduced the depth of Conformer-12 (BConformerR) to evaluate the effectiveness of the original architecture. Then, ResNet-152 and ResNet-101, as well as ViT-12 and ViT-9, were selected based on comparable parameters (Params) and multiply-accumulate operations (MACs) to Conformer-9 and Conformer-6 respectively. The F1 score was used as the primary evaluation metric for both linear and discontinuous epitope prediction.

4.3.2 Depth reduction

To evaluate the impact of model depth, we progressively reduced the number of layers in the Conformer architecture. As shown in Table 3, Conformer-12 achieves the highest F1 scores on both linear (0.672) and discontinuous (0.110) epitopes. Reducing depth to Conformer-9 leads to a moderate drop in performance, with linear and discontinuous F1

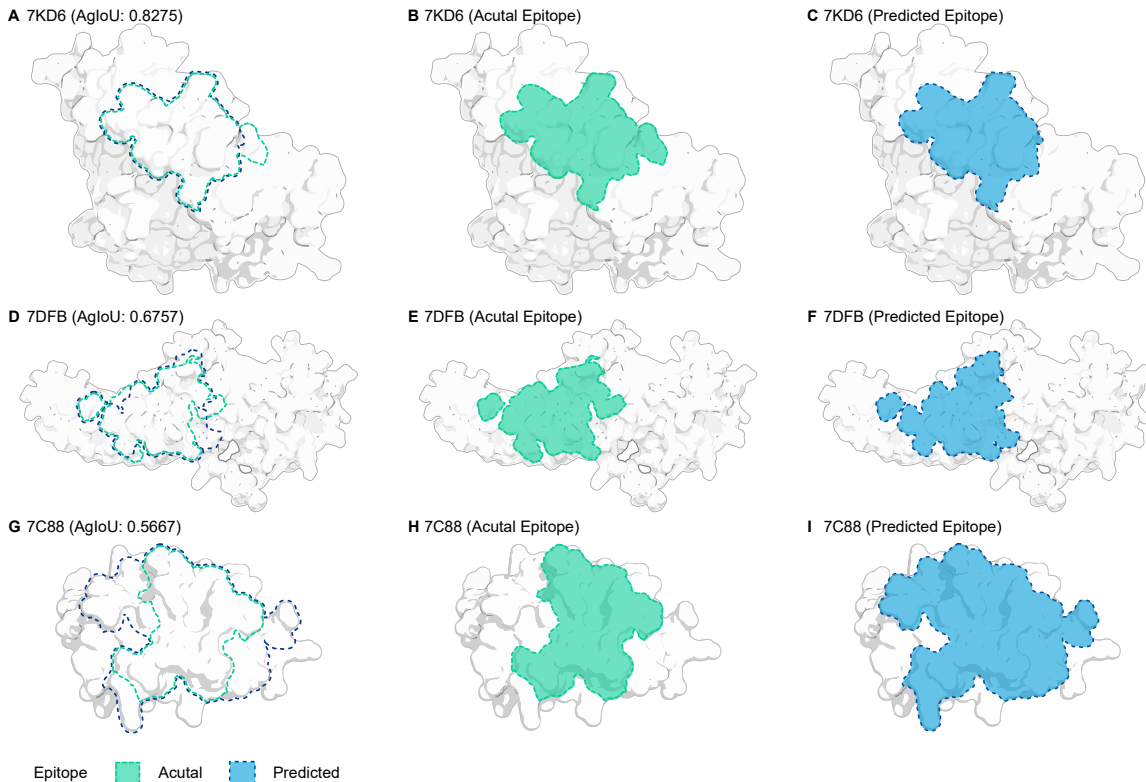


Figure 4: Structural visualization of epitopes predicted by BConformerR vs. actual epitopes. (A-C) Comparison of predicted and actual epitopes of 7KDB. Prediction is fully covered by the ground truth. (D-F) Comparison of predicted and actual epitopes of 7DFB. Prediction partially overlaps with the ground truth. (G-I) Comparison of predicted and actual epitopes of 7C88. Real epitopes are fully covered by the prediction.

scores decreasing by 4.0% (0.645) and 13.6% (0.095) respectively. Further reduction to Conformer-6 causes a more significant decline, especially in discontinuous epitope prediction, where the F1 score drops by 35.5% to 0.071. These demonstrate that our final model, BConformerR, achieves superior performance compared to shallower variants.

4.3.3 Conformer vs. CNN

Purely convolutional variants capture contiguous residue patterns efficiently and therefore achieve competitive scores on linear epitopes. However, their strictly local receptive field prevents them from modelling long-range residue couplings that dominate conformational epitopes. As shown in Table 3, ResNet-152 attains the highest linear F1 score (0.674) among all models, confirming its effectiveness on local patterns. However, its discontinuous F1 drops to 0.079, lower than Conformer-9 (0.095) and ViT-12 (0.086), indicating a weakness in capturing discontinuous dependencies.

By injecting a Transformer branch and exchanging information through FCUs, Conformer-9 achieves a discontinuous F1 score of 0.095, outperforming ResNet-152 (0.079), while maintaining a competitive linear F1 score of 0.645. This shows that integrating global context into convolutional layers can effectively improve discontinuous epitope prediction without sacrificing linear performance.

4.3.4 Conformer vs. ViT

Vision Transformer variants excel at aggregating sequence-wide information but lack explicit inductive bias for short-range motifs, often resulting in underfitting on linear stretches and noisy attention over densely packed regions. As shown in Table 3, ViT-9 achieves a discontinuous F1 of 0.082, surpassing ResNet-152 (0.079) and ResNet-101 (0.048). However, this comes at the cost of reduced performance on linear epitopes, where ViT-9 trails behind ResNet-101 (0.617 vs. 0.629).

Conformer mitigates this trade-off, as Conformer-9 outperforms ViT-12 on both linear (0.645 vs. 0.639) and discontinuous (0.095 vs. 0.086) F1 scores. Empirically, the hybrid design offers a more balanced solution for linear and discontinuous epitope prediction.

4.4 High-Confidence Predicted Structures

4.4.1 Predicted epitopes with high AgIoU

To visualize the prediction compared to the ground truth, we selected three antigen records from the test set with high AgIoU scores. Three overlap cases were shown in Figure 4: (1) the prediction is fully covered by the real epitopes (Fig. 4A-C), (2) the prediction partially overlaps with the real epitopes (Fig. 4D-F), (3) the real epitopes are entirely encompassed by the prediction (Fig. 4G-I).

5 Conclusion and Limitation

We present **BConformer**, a dual-branch Conformer model that integrates convolutional and self-attention mechanisms for residue-level prediction of both linear and conformational B-cell epitopes from antigen sequences. In addition to the architecture itself, two auxiliary contributions are worth noting: (i) an *adaptive logit-fusion* mechanism that automatically balances evidence from the CNN and Transformer branches, yielding a single, well-calibrated probability for each residue without extra post-processing; (ii) a detailed *performance analysis on both linear and discontinuous epitopes*, which also validates the complementary effectiveness of the CNN and Transformer branches. Benchmark evaluation demonstrates that our model consistently outperforms strong sequence- and structure-based baselines, particularly on the more difficult task of predicting conformational epitopes. The anticipated beneficiaries include rational vaccine design, diagnostic reagent development and antibody engineering pipelines.

Limitations. There are two notable limitations to this study. First, all training and test interfaces are derived from *in silico* AlphaFold-Multimer models; although this choice enlarges the dataset, it may introduce misoriented chains or misplaced atoms. Second, despite the size of our collection, antigen families and epitope types are imbalanced, which could bias both training and evaluation.

Acknowledgments

The computation resources in this study was sponsored by BayVax Biotech Limited. Y.-F. H. thanks support from the Major Program of the National Natural Science Foundation of China (92369201). The research was also supported by the National Key Research and Development Program of China (2021YFA0910700), the Health and Medical Research Fund, the Food and Health Bureau, The Government of the Hong Kong Special Administrative Region (COVID1903010, T-11-709/21-N) to J.-D.H. J.-D.H. also thanks the L & T Charitable Foundation, the Program for Guangdong Introducing Innovative and Entrepreneurial Teams (2019BT02Y198) and Shenzhen Key Laboratory for Cancer Metastasis and Personalized Therapy (ZDSYS20210623091811035) for their support.

References

- [1] Edgar Ernesto Gonzalez Kozlova, Loïc Cerf, Francisco Santos Schneider, Benjamin Thomas Viart, Christophe NGuyen, Bethina Trevisol Steiner, Sabrina de Almeida Lima, Franck Molina, Clara Guerra Duarte, Liza Felicori, et al. Computational b-cell epitope identification and production of neutralizing murine antibodies against atroxlysin-i. *Scientific reports*, 8(1):14904, 2018.
- [2] Rui Jia, Gaiping Zhang, Yilin Bai, Hongliang Liu, Yumei Chen, Peiyang Ding, Jingming Zhou, Hua Feng, Mingyang Li, Yuanyuan Tian, et al. Identification of linear b cell epitopes on cd2v protein of african swine fever virus by monoclonal antibodies. *Microbiology Spectrum*, 10(2):e01052-21, 2022.
- [3] Danniele L Vale, Amanda S Machado, Fernanda F Ramos, Daniela P Lage, Camila S Freitas, Daysiane de Oliveira, Nathalia C Galvani, Gabriel P Luiz, Mirian I Fagundes, Bruna B Fernandes, et al. Evaluation from a b-cell epitope-based chimeric protein for the serodiagnosis of tegumentary and visceral leishmaniasis. *Microbial Pathogenesis*, 167:105562, 2022.
- [4] Ivan Talucci and Hans M Maric. Epitope landscape in autoimmune neurological disease and beyond. *Trends in pharmacological sciences*, 45(9):768-780, 2024.

- [5] Alexandra R Dvorscek, Craig I McKenzie, Vera C Stäheli, Zhoujie Ding, Jacqueline White, Stewart A Fabb, Leonard Lim, Kristy O’Donnell, Catherine Pitt, Daniel Christ, et al. Conversion of vaccines from low to high immunogenicity by antibodies with epitope complementarity. *Immunity*, 57(10):2433–2452, 2024.
- [6] Esmaeil Roohparvar Basmenj, Susan Radman Pajhouh, Afsane Ebrahimi Fallah, Elmira Rahimi, Hossein Atighy, Shadan Ghiabi, Shamim Ghiabi, et al. Computational epitope-based vaccine design with bioinformatics approach; a review. *Heliyon*, 11(1), 2025.
- [7] Gisela Brändén and Richard Neutze. Advances and challenges in time-resolved macromolecular crystallography. *Science*, 373(6558):eaba0954, 2021.
- [8] Pawel Rubach, Karolina A Majorek, Michal Gucwa, Krzysztof Murzyn, Alexander Wlodawer, and Wladek Minor. Advances in cryo-electron microscopy (cryoem) for structure-based drug discovery. *Expert Opinion on Drug Discovery*, (just-accepted), 2025.
- [9] Line Ledsgaard, Anne Ljungars, Charlotte Rimbault, Christoffer V Sørensen, Tulika Tulika, Jack Wade, Yessica Wouters, John McCafferty, and Andreas H Laustsen. Advances in antibody phage display technology. *Drug Discovery Today*, 27(8):2151–2169, 2022.
- [10] Tatiana I Shashkova, Dmitriy Umerenkov, Mikhail Salnikov, Pavel V Strashnov, Alina V Konstantinova, Ivan Lebed, Dmitriy N Shcherbinin, Marina N Asatryan, Olga L Kardymon, and Nikita V Ivanisenko. Sema: Antigen b-cell conformational epitope prediction using deep transfer learning. *Frontiers in immunology*, 13:960985, 2022.
- [11] Nikita V Ivanisenko, Tatiana I Shashkova, Andrey Shevtsov, Maria Sindeeva, Dmitriy Umerenkov, and Olga Kardymon. Sema 2.0: web-platform for b-cell conformational epitopes prediction using artificial intelligence. *Nucleic Acids Research*, 52(W1):W533–W539, 2024.
- [12] Jens Erik Pontoppidan Larsen, Ole Lund, and Morten Nielsen. Improved method for predicting linear b-cell epitopes. *Immunome research*, 2:1–7, 2006.
- [13] Martin Closter Jespersen, Bjoern Peters, Morten Nielsen, and Paolo Marcatili. Bepipred-2.0: improving sequence-based b-cell epitope prediction using conformational epitopes. *Nucleic acids research*, 45(W1):W24–W29, 2017.
- [14] Joakim Nøddeskov Clifford, Magnus Haraldson Høie, Sebastian Deleuran, Bjoern Peters, Morten Nielsen, and Paolo Marcatili. Bepipred-3.0: Improved b-cell epitope prediction using protein language models. *Protein Science*, 31(12):e4497, 2022.
- [15] Chen Zhou, Zikun Chen, Lu Zhang, Deyu Yan, Tiantian Mao, Kailin Tang, Tianyi Qiu, and Zhiwei Cao. Seppa 3.0—enhanced spatial epitope prediction enabling glycoprotein antigens. *Nucleic acids research*, 47(W1):W388–W394, 2019.
- [16] Zeming Lin, Halil Akin, Roshan Rao, Brian Hie, Zhongkai Zhu, Wenting Lu, Allan dos Santos Costa, Maryam Fazel-Zarandi, Tom Sercu, Sal Candido, et al. Language models of protein sequences at the scale of evolution enable accurate structure prediction. *BioRxiv*, 2022:500902, 2022.
- [17] Zeming Lin, Halil Akin, Roshan Rao, Brian Hie, Zhongkai Zhu, Wenting Lu, Nikita Smetanin, Robert Verkuil, Ori Kabeli, Yaniv Shmueli, et al. Evolutionary-scale prediction of atomic-level protein structure with a language model. *Science*, 379(6637):1123–1130, 2023.
- [18] Jens Vindahl Kringelum, Claus Lundegaard, Ole Lund, and Morten Nielsen. Reliable b cell epitope predictions: impacts of method development and improved benchmarking. *PLoS computational biology*, 8(12):e1002829, 2012.
- [19] Magnus Haraldson Høie, Frederik Steensgaard Gade, Julie Maria Johansen, Charlotte Würtzen, Ole Winther, Morten Nielsen, and Paolo Marcatili. Discotope-3.0: improved b-cell epitope prediction using inverse folding latent representations. *Frontiers in immunology*, 15:1322712, 2024.
- [20] Jérôme Tubiana, Dina Schneidman-Duhovny, and Haim J Wolfson. Scannet: an interpretable geometric deep learning model for structure-based protein binding site prediction. *Nature Methods*, 19(6):730–739, 2022.
- [21] Bruna Moreira da Silva, YooChan Myung, David B Ascher, and Douglas EV Pires. epitope3d: a machine learning method for conformational b-cell epitope prediction. *Briefings in Bioinformatics*, 23(1), 2022.
- [22] Johan Nilvebrant, Niklas Berndt Thalén, Johan Rockberg, and Magdalena Malm. An overview of epitopes and methods for antibody epitope mapping. *Epitope Mapping Protocols*, pages 1–11, 2025.
- [23] Anmol Gulati, James Qin, Chung-Cheng Chiu, Niki Parmar, Yu Zhang, Jiahui Yu, Wei Han, Shibo Wang, Zhengdong Zhang, Yonghui Wu, et al. Conformer: Convolution-augmented transformer for speech recognition. *arXiv preprint arXiv:2005.08100*, 2020.

- [24] Zhiliang Peng, Wei Huang, Shanzhi Gu, Lingxi Xie, Yaowei Wang, Jianbin Jiao, and Qixiang Ye. Conformer: Local features coupling global representations for visual recognition. In *Proceedings of the IEEE/CVF international conference on computer vision*, pages 367–376, 2021.
- [25] Cao Ying, Miao Qi-Guang, Liu Jia-Chen, and Gao Lin. Advance and prospects of adaboost algorithm. *Acta Automatica Sinica*, 39(6):745–758, 2013.
- [26] Jin Su, Chenchen Han, Yuyang Zhou, Junjie Shan, Xibin Zhou, and Fajie Yuan. Saprot: Protein language modeling with structure-aware vocabulary. *BioRxiv*, pages 2023–10, 2023.
- [27] Chloe Hsu, Robert Verkuil, Jason Liu, Zeming Lin, Brian Hie, Tom Sercu, Adam Lerer, and Alexander Rives. Learning inverse folding from millions of predicted structures. In *International conference on machine learning*, pages 8946–8970. PMLR, 2022.
- [28] Joakim Nøddeskov Clifford, Eve Richardson, Bjoern Peters, and Morten Nielsen. Abepitope-1.0: Improved antibody target prediction by use of alphafold and inverse folding. *Science Advances*, 11(24):eadu1823, 2025.
- [29] Jing Sun, Tianlei Xu, Shuning Wang, Guoqing Li, Di Wu, and Zhiwei Cao. Does difference exist between epitope and non-epitope residues? *Immunome research*, 7(3):1, 2011.
- [30] Saba Ferdous, Sebastian Kelm, Terry S Baker, Jiye Shi, and Andrew CR Martin. B-cell epitopes: Discontinuity and conformational analysis. *Molecular immunology*, 114:643–650, 2019.
- [31] Kaiming He, Xiangyu Zhang, Shaoqing Ren, and Jian Sun. Deep residual learning for image recognition. In *Proceedings of the IEEE conference on computer vision and pattern recognition*, pages 770–778, 2016.
- [32] Alexey Dosovitskiy, Lucas Beyer, Alexander Kolesnikov, Dirk Weissenborn, Xiaohua Zhai, Thomas Unterthiner, Mostafa Dehghani, Matthias Minderer, Georg Heigold, Sylvain Gelly, et al. An image is worth 16x16 words: Transformers for image recognition at scale. *arXiv preprint arXiv:2010.11929*, 2020.

Appendix

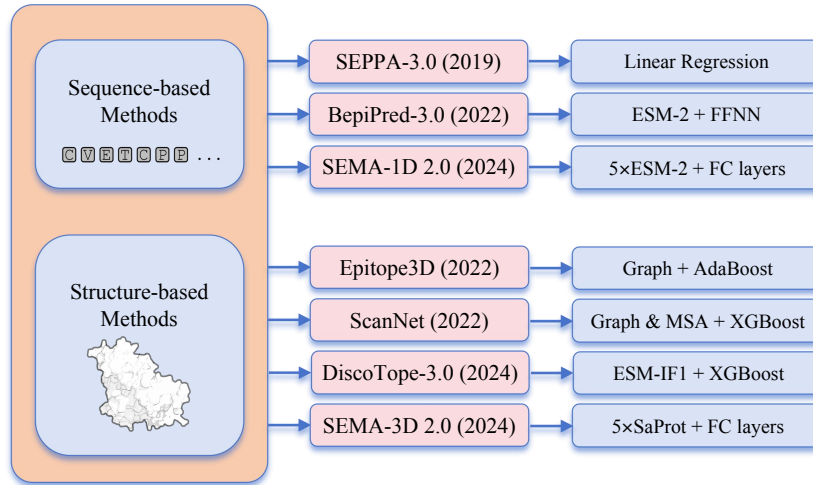


Figure 5: Related work on epitope prediction methods. FFNN denotes feedforward neural network; FC layers denotes fully connected layers; MSA denotes multiple sequence alignment results.

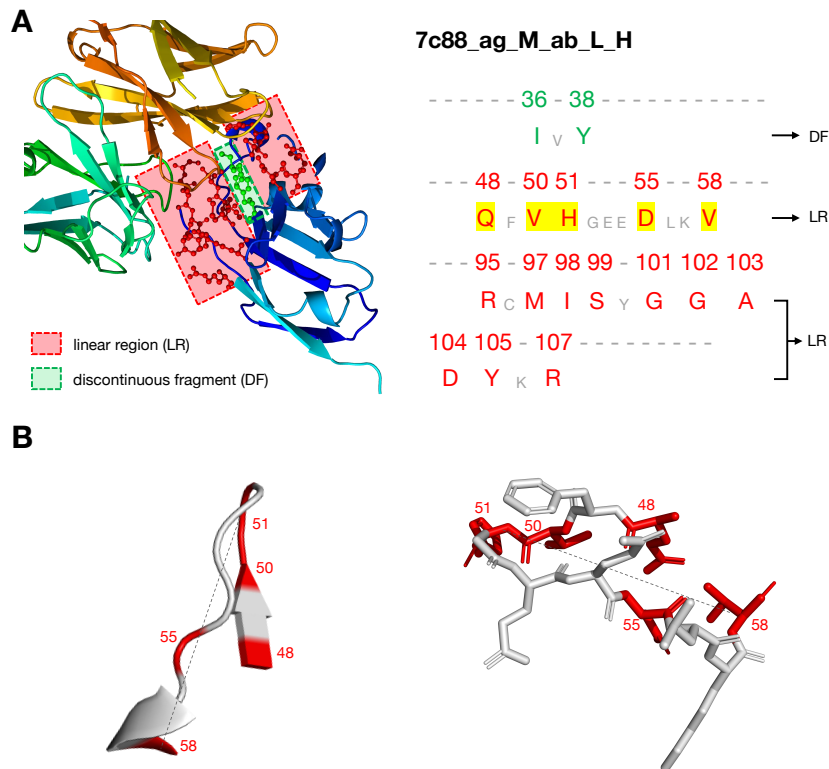


Figure 6: Linear regions and discontinuous fragments. (A) (Left) The blue structure represents antigen 7c88, and the light green and light orange correspond to parts of the two antibody heavy chains; Linear regions are marked with red rectangles, and discontinuous fragments with green. (Right) Residues highlighted with numbers indicate epitopes. (B) A linear region of 7c88. Gap size of up to three non-contacting residues is chosen for a linear region on the basis of the structure of α -helices.

A Antibody-agnostic prediction methods

We summarize widely-used epitope prediction methods, categorized into sequence-based and structure-based approaches, as shown in Figure 5. Methods with the latest versions are summarized along with their data representation strategies and classifiers.

B Linear Regions and Discontinuous Fragments

Regions are defined as linear stretches of antigen sequence having at least three antibody-contacting residues (Fig. 6A). Gaps between contacting residues are allowed, and a gap size of up to three non-contacting residues is chosen on the basis of the structure of α -helices, which enables residues on the same helical face to be included (Fig. 6B). Fragments, which do not contain enough antibody-contacting residues to qualify as a region (less than three), are considered discontinuous in our study (Fig. 6A).

C Dataset

C.1 Structure prediction

We initially obtained 1730 antibody–antigen (Ab–Ag) FASTA files from AbEpiTope-1.0. However, due to the limited computational time and the large size of certain input sequences, we only processed 1300 complexes using the AlphaFold2 Multimer v3. Each of these 1300 complexes was modeled with 5 seeds, 6 models and 3 recycles, generating 30 structures per complex.

C.2 Epitope statistics

The final dataset consists of 1180 Ab–Ag complexes, which contains a total of 1432 antigen chains and 2320 antibody chains. Epitopes were identified using a 4 Å distance cutoff between antigen and antibody residues. After classifying the epitopes into linear and discontinuous types, we found 2388 linear regions comprising 15,886 residues, and 2632 discontinuous fragments comprising 3574 residues.

D Performance Metrics

The performance metrics used in this study include Precision, Recall, F1-score, Antigen-level intersection over union (AgIoU), Matthews correlation coefficient (MCC) and Pearson correlation coefficient (PCC), whose definitions are given as follows:

$$\begin{aligned}
 \text{Precision} &= \frac{TP}{TP + FP}, \\
 \text{Recall} &= \frac{TP}{TP + FN}, \\
 \text{F1} &= \frac{2TP}{2TP + FP + FN}, \\
 \text{AgIoU} &= \frac{TP}{TP + FP + FN}, \\
 \text{MCC} &= \frac{TP \cdot TN - FP \cdot FN}{\sqrt{(TP + FP)(TP + FN)(TN + FP)(TN + FN)}}, \\
 \text{PCC} &= \frac{\sum_{i=1}^n (y_i - \bar{y})(\hat{y}_i - \bar{\hat{y}})}{\sqrt{\sum_{i=1}^n (y_i - \bar{y})^2} \sqrt{\sum_{i=1}^n (\hat{y}_i - \bar{\hat{y}})^2}},
 \end{aligned} \tag{9}$$

where TP , TN , FP and FN denote the number of true positives, true negatives, false positives and false negatives, respectively; y_i and \hat{y}_i represent the ground-truth and predicted values, while \bar{y} and $\bar{\hat{y}}$ denote their means. The relationships between these metrics are given as:

$$F1 = \frac{2 \cdot \text{Precision} \cdot \text{Recall}}{\text{Precision} + \text{Recall}} = \frac{2 \cdot \text{AgIoU}}{1 + \text{AgIoU}},$$

$$\text{AgIoU} = \frac{2 \cdot F1}{2 - F1}.$$
(10)

E Evaluation and Comparison

E.1 Evaluation

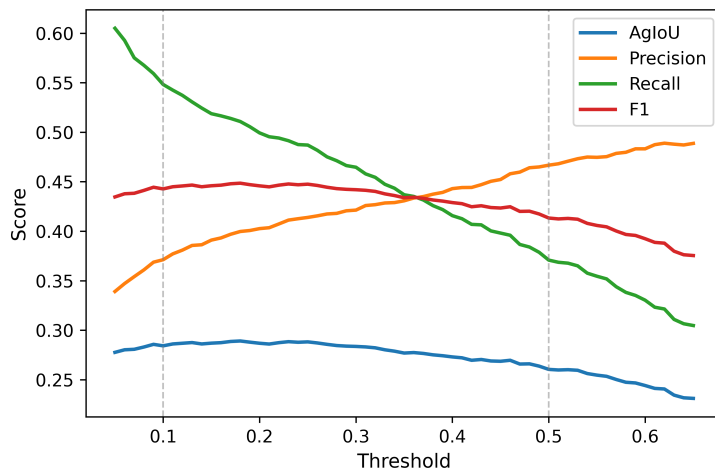


Figure 7: Metrics across thresholds on the test set of 100 antigens.

BConformerR was evaluated at various thresholds on 100 antigen records. As shown in Figure 7, the range between 0.1 and 0.5—highlighted by gray dashed lines—represents the region where precision, recall, F1 score and AgIoU perform well. Notably, the F1 score peaks around 0.44 when thresholds are set between 0.1 and 0.3.

E.2 Baseline methods

Thresholds for all baselines were adjusted to reflect their best scoring behavior, ensuring a fair comparison with BConformerR in the blind test. We observed that SEPPA-3.0 performs better under a low decision threshold (around 0.1). For SEMA-1D 2.0, which defines epitope residues using an 8 Å distance cutoff, the predicted scores tend to be higher; thus, we adopted a threshold of 0.5 above its default of 0.351. Moreover, although the default threshold of BepiPred-3.0 is 0.1512, we found that a slightly higher value around 0.2 led to better balance between precision and recall on our test set.

F Ablation

F.1 ViT

Model	Embed Dimension	Seq Length	Patch Size	Depth	Heads	MLP Ratio
ViT-9	1536	1024	1	9	12	2.0
ViT-12	1536	1024	1	12	12	2.0

Table 4: ViT-1D variants used in ablation study.

We conducted ablation studies on two variants of the ViT-1D model differing in depth: ViT-9 and ViT-12. As shown in Table 4, both models share the same embedding dimension (1536), input sequence length (1024), patch size (1), number of attention heads (12), and MLP expansion ratio (2.0). The only difference is the number of transformer encoder layers.

F.2 Resnet

Stage	Output Channels	Kernel Size	Resnet-101	Resnet-152
input	1280	-	-	-
stem	320	7	-	-
layer1	640 (160×4)	3	3	3
layer2	1280 (320×4)	3	4	8
layer3	2560 (640×4)	3	23	36
layer4	5120 (1280×4)	3	3	3
classifier	2	1	-	-

Table 5: ResNet-1D architectures used in ablation study.

We employed two variants of the ResNet-1D backbone in the ablation studies: ResNet-101 and ResNet-152. As shown in Table 5, both models accept input feature maps with 1280 channels and begin with an initial convolutional layer producing 320 channels. The networks consist of four residual stages of bottlenecks with the expansion factor of 4, each stage starting by downsampling the channel dimension to half. The difference lies in the number of bottleneck blocks per stage. ResNet1D-101 contains [3, 4, 23, 3] blocks across the four layers, while ResNet1D-152 is deeper with [3, 8, 36, 3] blocks. The final output is projected to the target classes through a 1×1 convolutional layer.

G Data and Code Availability

The data and code are available at <https://github.com/Jerry-alt19/BConformerR>.